Research article

JGS
Journal of the Geological Society

https://doi.org/10.1144/jgs2023-042 | Vol. 181 | 2023 | jgs2023-042

Using ground-penetrating radar to investigate deposits from the Storegga slide tsunami and other sand sheets in the Shetland Islands, UK

L. Buck and C. S. Bristow*

Department of Earth and Planetary Sciences, Birkbeck, University of London, Malet Street, London WC1E 7HX, UK
LB, 0009-0001-9052-5518; CSB, 0000-0002-6275-4591
*Correspondence: c.bristow@ucl.ac.uk

Abstract: We use ground-penetrating radar (GPR) to investigate the geometry, inland extent and continuity of sand layers interpreted as tsunami deposits in the Shetland Islands, UK. Four sites where sand layers within peat deposits have been recorded in previous studies are used to provide ground truth. In addition, we describe survey results from one site where deposits are not exposed to test the potential of GPR to identify candidate tsunami deposits in areas that are not well documented. Sand layers can be clearly imaged at all five locations because they are interbedded with peat and the contrast in lithology gives a good reflection on GPR profiles, even very thin sand layers, <1 cm thick, that are beneath the theoretical resolution of the GPR. 2D and 3D surveys show that tsunami deposits appear to drape a buried topography. Most sand layers form continuous reflections, although some gaps are attributed to later erosion, most likely by streams. Sand layers have been traced up to 150 m inland and 10 m above the present shoreline, which is consistent with data from boreholes. If a similar sized event occurred today, it would have a devastating impact on the Shetland Islands.

Received 13 April 2023; **revised** 24 October 2023; **accepted** 15 November 2023

The vulnerability of communities to tsunamis increases as coastal populations and economic pressures increase (Li *et al.* 2018; Engel *et al.* 2020; Alhamid *et al.* 2022; Tursina *et al.* 2022). Hazard management is based on a knowledge of the frequency and magnitude of past events in a certain area (Satake and Atwater 2007; Goto *et al.* 2014; Coppola 2020). As a result, studies of the deposits from palaeotsunamis are crucial in decreasing vulnerability in coastal communities (Minoura *et al.* 2001; Jin and Lin 2011). However, it can be challenging to identify tsunami deposits (Kortekaas and Dawson 2007; Switzer and Jones 2008; Costa and Andrade 2020). Ground-penetrating radar (GPR) provides a non-invasive, high-resolution method of imaging the shallow subsurface, making it a potentially useful tool in identifying and mapping tsunami deposits.

The Shetland Islands have been described as an ideal field laboratory for tsunami geoscience (Dawson *et al.* 2020) and the deposits of three Holocene tsunami events have been described there (Bondevik *et al.* 2005): the Storegga tsunami at 8.120–8.175 cal ka BP (Bondevik *et al.* 2012); the Garth tsunami at *c.* 5.500 cal ka BP; and the Dury Voe event at *c.* 1.500 cal ka BP (Bondevik *et al.* 2005), although Engel *et al.* (2023) suggest a slightly younger age for the Dury Voe event of *c.* 1.400 cal ka BP. Deposits from the tsunamis have been found in Norway (Bondevik *et al.* 1997*a*, *b*; Bondevik and Svendsen 1998), mainland Scotland (Smith *et al.* 1992, 2004; Dawson and Smith 1997; Long *et al.* 2016), the Shetland Islands (Smith *et al.* 2004; Bondevik *et al.* 2005), the Faroe Islands (Grauert *et al.* 2001) and Greenland (Wagner *et al.* 2007).

The Storegga and Garth tsunamis are linked to the Storegga slide, where slope failure on the Norwegian shelf edge produced one of the biggest recorded submarine landslides (Fig. 1). Radiocarbon dating supports the correlation of the Storegga tsunami and the submarine landslide (Bondevik *et al.* 2012). The Garth tsunami is linked to headwall collapse of the Storegga slide, which has been described as a candidate for the Garth tsunami (Bondevik *et al.* 2005). The origin of the Dury Voe event remains to be determined. Potential tsunami sources around the North Atlantic were discussed by ten Brink *et al.* (2014) and include submarine landslides, volcano flank collapse, earthquakes and atmospheric disturbances (meteotsunamis). Another source of coastal sand sheets is storms and there is a sedimentary record of high-magnitude storm events in the Shetland Islands (Hess *et al.* 2023). Storm and tsunami deposits might be distinguished by detailed sedimentology (Kortekaas and Dawson 2007; Switzer and Jones 2008; Phantuwongraj and Choowong 2012; Costa and Andrade 2020), but it is unlikely that they could be distinguished by GPR alone and caution is required when attributing sand layers to specific events.

GPR has been used to detect tsunami deposits in various places around the world, including the USA (Jol and Peterson 2006), Spain (Koster *et al.* 2013; Koster and Reicherter 2014), Greece (Koster *et al.* 2013), Oman (Koster *et al.* 2014), Thailand (Gourmanis *et al.* 2015), Sri Lanka (Premasiri *et al.* 2015) and Japan (Takamura *et al.* 2016; Takeda *et al.* 2018; Sawai *et al.* 2023). GPR has not previously been used to detect Storegga slide tsunami deposits. We carried out GPR surveys in the Shetland Islands to characterize the deposits created by these tsunamis. Initial surveys were undertaken in areas where deposits have been described by Bondevik *et al.* (2003, 2005), Smith *et al.* (2004) and Dawson *et al.* (2020) to establish the reflection characteristics of tsunami deposits in areas with ground truth. Once the signature of the tsunami deposits within the GPR data had been identified, we used GPR to explore a prospective site where there is no previous record of tsunami deposits.

The aims of this study are: (1) to test the hypothesis that GPR can be used to image tsunami sand layers in peat; (2) to determine the extent and continuity of tsunami sand layers inland and up-slope (run-up) using GPR; (3) to image the geometry of tsunami sand layers in two and three dimensions; and (4) to explore an area where tsunami deposits have not previously been recorded. This paper describes the results from five sites in the Shetland Islands: the Ayre

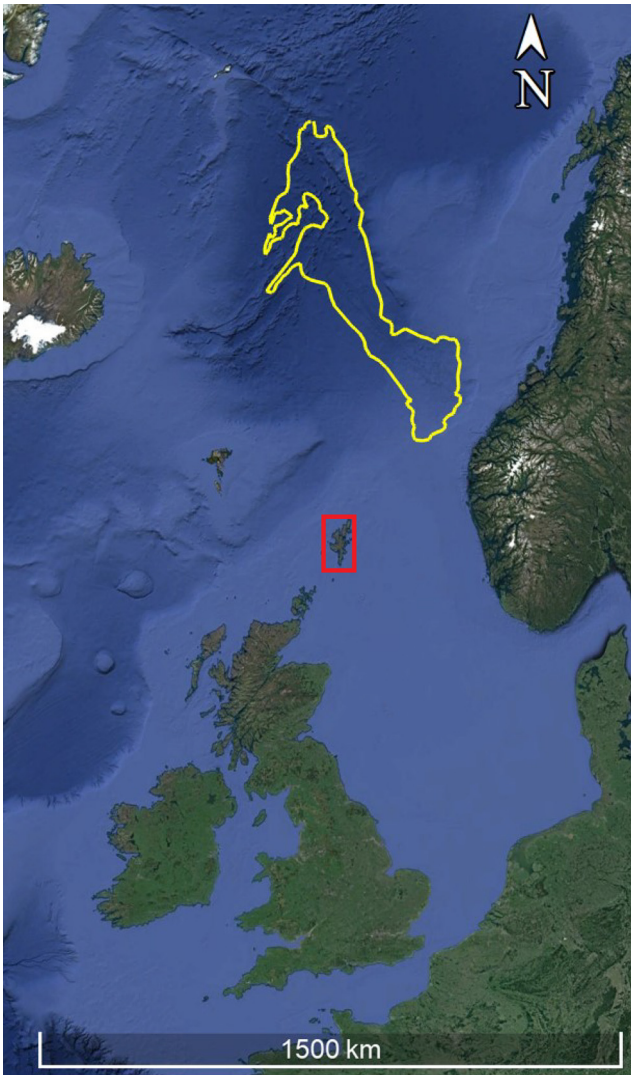

Fig. 1. Annotated satellite image showing the Storegga slide outline in yellow, with the Shetland Islands shown in the red box. The Storegga slide is one of the largest submarine landslides ever mapped. Source: location of Storegga slide after Bondevik *et al.* (2005); satellite image from Google Earth™ Data SIO, NOAA, US Navy, NGA, GEBCO, image Landsat/Copernicus, image US Geological Survey.

of Dury and Scatsta Voe on the island of Mainland and Basta Voe, Grimister and Whale Firth on the island of Yell (Fig. 2).

Method

We used a Sensors and Software Pulse EKKO ultra GPR system with 100, 200 and 500 MHz antennas. We tested different configurations at Scatsta Voe with the 100 and 200 MHz antennas and determined that 200 MHz antennas spaced 1 m apart in a parallel broadside configuration with a step size of 0.2 m gave a good balance of resolution and depth of penetration. The 500 MHz antennas were at a fixed separation of 0.23 m with a step size of 0.1 m. The GPR data processing was performed using Sensors and Software EKKO Project 5 software. The processing steps included an SEC gain (Max 250) and topographic correction. An FK migration was applied using a velocity of 0.035 m/ns. The velocity used for depth corrections in Shetland is 0.035 m/ns. The velocity was determined from CMP surveys at each site, curve-fitting to hyperbolas and correlation with boreholes through the peat, where velocity calculations ranged from 0.037 to 0.04 m/ns. These velocities are consistent with published velocities for peat (Proulx-McInnis *et al.* 2013; Parry *et al.* 2014). Using a velocity of 0.035 m/ns and assuming a resolution of one-quarter of the wavelength gives a theoretical depth resolution of 0.1 m for the 100 MHz antennas, 0.05 m for the 200 MHz antennas and 0.02 m for the 500 MHz antennas. Elevation data for topographic correction were measured at 1 m intervals along the profiles using a Leica NA320 automatic level with elevations corrected to Ordnance Datum (OD) by surveying local high-water tide lines and applying a correction from Admiralty tide tables.

The peat was effectively saturated at the time of the GPR and topographic surveys in May 2019 and May 2021, with the water table at or within 10 cm of the surface. Where possible, the GPR profiles followed relatively smooth interfluves, avoiding streams and areas where the peat might have been disturbed by peat flows or peat cutting, which leave visible scars on the landscape. Auger boreholes were made using an Eijkelkamp hand auger with a stainless-steel peat sampler/gouge auger. To create the 3D

Fig. 2. Location of study sites (red circles) and critical infrastructure, including the oil terminal at Sullom Voe, the airport at Sumburgh and the island's capital Lerwick (open squares) in the Shetland Islands. Source: satellite image from Google Earth™ data SIO, NOAA, US Navy, NGA, GEBCO, image Landsat/Copernicus.

morphology of the sand layer at Ayre of Dury, depth values for the sand layer were picked at 0.5 m intervals on the GPR profiles. Plotly Chart Studio, an online tool used to create graphs in Python, was then used to create a 3D surface area graph to display the sand layer in 3D.

Study sites

Ayre of Dury

The Ayre of Dury is a shingle beach located at the southernmost point of the Dury Voe inlet, a west-facing inlet in NE Mainland [60° 19′ 24.89″ N, 01° 09′ 56.95″ W]. The tsunami deposits here were described by Bondevik *et al.* (2005) as being 1–5 cm thick and composed of fine- to medium-grained sand with a sharp lower boundary. The sand is exposed in natural sections eroded into peat deposits south of the spit (Fig. 3) and we also noted a large pebble associated with the sand layer. The deposit has been traced for up to 5.6 m above the current high tide level and thins inland (Bondevik *et al.* 2005). It has been dated to between 1.540–1.820 and 1.290–1.420 cal ka BP and has been ascribed to the Dury Voe event (Bondevik *et al.* 2005). The origin of the event is not certain because it appears to be younger than the dates for the Storegga slides reported by Haflidason *et al.* (2005) and the origin of the sand sheet remains to be determined. We investigated the geometry of the tsunami sand layer at the Ayre of Dury in 3D using a grid of 15 lines, each 10 m long, spaced 0.5 m apart and covering an area 7 m wide and 10 m long (Fig. 3). For each line, 500 MHz antenna were used with a pre-set separation of 0.23 m and a 0.1 m step size.

Basta Voe

Basta Voe is a NNW–SSE-trending funnel-shaped inlet located in the north of Yell [60° 19′ 26.60″ N, 01° 10′ 3.51″ W]. The western coast of the inlet is characterized by low peat cliffs. Exposures in these cliffs and adjacent peat cuttings show sand horizons interbedded with peat overlying glacial deposits (Dawson *et al.* 2006). Dawson *et al.* (2006) described three sand layers, two of which are of limited extent, outcropping for 10–15 m along the coast and occupying an area <40–50 m^2, interpreting them as probable storm deposits. The third, younger, sand layer is more extensive, outcropping over 2 km and traceable up to an elevation of 9 m OD (Dawson *et al.* 2006). A storm hypothesis was rejected for the third sand layer and Dawson *et al.* (2006) suggest that it is a tsunami deposit, dated to 1.300–1.570 cal ka BP, similar in age to the Dury Voe event described at the Ayre of Dury by Bondevik *et al.* (2005).

Two GPR profiles were collected at Basta Voe. Line A–B was collected with 200 MHz antennas spaced 1 m apart and a step size of 0.5 m. The line was 110 m long and followed the coastline, initially north–south and then swinging around towards the west. Line C was 27 m long and perpendicular to the coast on the western side of Basta Voe (Fig. 4). Here, a thin sand layer is exposed in peat cuttings and can be seen pinching out inland. Line C was collected parallel to the outcrop and was used to determine the limits of resolution of a sand layer by GPR using 500 MHz antennas with a pre-set separation of 0.23 m and a 0.1 m step size. Along line C, a peat cutting gouge auger was used to collect cores up to 1 m depth at 5 m intervals, with the exception of the last borehole, which was taken at 27.5 m. The thickness and depth of the sand layer were measured in the cores.

Scatsta Voe

Scatsta Voe is a small inlet on the southern shore of Yell Sound [60° 26′ 15.66″ N, 01° 16′ 44.91″ W], within Sullom Voe on Mainland and located immediately NE of Scatsta Airport and SW of Sella Ness Harbour and Sullom Voe oil terminal. Sullom Voe is the largest inlet in the Shetland Islands and Scatsta Voe is one of many voes (inlets), houbs (small land-locked bays or lagoons) and headlands found in the sheltered middle section. The presence of a sand layer at Scatsta Voe was described by Smith (1993), who reported the sand layer outcropping at 3.84 m OD and traced it inland in boreholes to an elevation of 12.45 m OD. Radiocarbon dates from Smith (1993) give ^{14}C dates of 5.700 ± 0.045 (6.635–6.355 cal ka BP; Smith *et al.* 2004) beneath the sand layer and 3.815 ± 0.045 (4.406–4.087 cal ka BP Smith *et al.* 2004) above. Additional radiocarbon dates from outcrops around Sullom Voe include radiocarbon dating of seeds beneath the sand layer of 7.120 ± 0.060 ^{14}C ka BP (8.107–7.791 cal ka BP; Smith *et al.* 2004) and 7.025 ± 0.060 ^{14}C ka BP (7.957–7.699 cal ka BP Smith *et al.* 2004) from a stick immediately above the sand layer (Bondevik *et al.* 2003). Bondevik *et al.* (2003) suggested that the bulk radiocarbon ages reported by Smith (1993) are 1500–2000 years too young, possibly contaminated by younger carbon, most likely caused by root penetration.

Two survey lines were taken at Scatsta Voe on either side of the road, the locations of which are shown in Figure 5. Line A–A′ is 40 m long and started 5 m NW of a small waterfall where the tsunami sand is exposed by the nearby unnamed stream and ends at the coast. The profile was repeated four times with a range of antenna frequencies and survey configurations (Table 1) to determine which combination of frequency, step size and antenna separation would best image the tsunami deposit. Line B–B′ is on the other side of the road and is 90 long, starting 3 m from the fence

Fig. 3. Satellite images of the Ayre of Dury at the southern end of Dury Voe on the east coast of Mainland. The right-hand image shows the location of the grid, with parallel lines A–N spaced 0.5 m apart and covering an area 7 m wide and 10 m long. The tsunami sand layer is exposed in a natural section along the south side of the outcrop. Source: satellite image from Google Earth™ Image © 2023 Maxar Technologies.

Fig. 4. Satellite image of Basta Voe showing the locations of the ground-penetrating radar profiles A–B and C–C′. Source: satellite image from Google Earth™, image Landsat/Copernicus, image © 2023 Maxar Technologies.

and ending at a channel eroded into the peat *c.* 175 m inland. For line B, 200 MHz antennas were used with a separation of 1 m and a step size of 0.2 m.

Whale Firth

Whale Firth is a north-facing voe on the western side of Yell [60° 36′ 17.62″ N, 01° 07′ 12.44″ W]. The firth is north–south-oriented, but has a bend roughly halfway down the inlet where it becomes NW–SE-oriented. A low cliff *c.* 50 m long exposes a section of peat overlying glacial till with one obvious sand layer of varying thickness between 0.12 and 0.01 m (Fig. 6). The sand layer has a sharp erosive base and thickens and thins along-strike. The sand varies between granule and fine sand in size and is locally graded.

Table 1. GPR antenna set-up for repeat surveys at Scatsta A–A′ to determine the optimum set-up for the depth of penetration and resolution (results shown in Fig. 12)

Survey	Antenna frequency (MHz)	Separation (m)	Step size (m)
Scatsta A1	500	0.23	0.1
Scatsta A.2	200	0.5	0.1
Scatsta A.3	200	1.0	0.2
Scatsta A.4	100	1.0	0.25

At outcrop, the thickness changes in the sand layer are lens-like (Fig. 6), but this is possibly a function of compaction, with the original sand layer thickening into erosional hollows and increased compaction pushing the top of the bed down where the sand is thinner. The presence of small faults supports compaction deformation. The sand layer is described in a British Geological Survey report (Tappin *et al.* 2015), which notes similarities between the appearance of the sand layer at Whale Firth and other Storegga tsunami outcrops. However, there is a radiocarbon age of 4.760 ± 0.030 cal ka BP from a twig at the top of the sand layer (Tappin *et al.* 2015). Tappin *et al.* (2015) discussed the significance of this radiocarbon age, which does not match the age of the early Holocene Storegga tsunami, and concluded that it could represent a mid-Holocene tsunami or contamination from younger carbon. The age of this sand layer remains to be properly determined, but is closest in age to the Garth tsunami.

At Whale Firth, the GPR profile starts on top of the cliff immediately above the outcrop and extends inland, up-slope in a southerly direction avoiding streams where erosion might have occurred (Fig. 6). The profile is 156 m long with an antenna frequency of 200 MHz, a step size of 0.2 m and an antenna separation of 1 m. Three boreholes were taken along the line at 45, 77 and 110 m to depths of 3, 3 and 2.25 m, respectively.

Grimister

Grimister is located part way down Whale Firth [60° 37′ 09.30″ N, 01° 09′ 04.03″W] and lies within a valley that is a continuation of the outer north–south section of the firth (Fig. 7), roughly 2.5 km closer to the sea than the site at Whale Firth. The Burn of Buster flows into the sea at Grimister. There is a small gravel beach, but, unlike at the other locations, there is no outcrop. Instead, the valley floor is a water-saturated bog. The British Geological Survey report (Tappin *et al.* 2015) indicates that an auger borehole was made at

Fig. 5. Satellite images of Sullom Voe, including Sullom Voe oil terminal, the airport at Scatsta and Sella Ness Harbour. The locations of the ground-penetrating radar profiles A–A′ and B–B′ either side of the B9076 road are shown in the rifgt-hand image. Source: Google Earth™, image © 2023 CNES/Airbus.

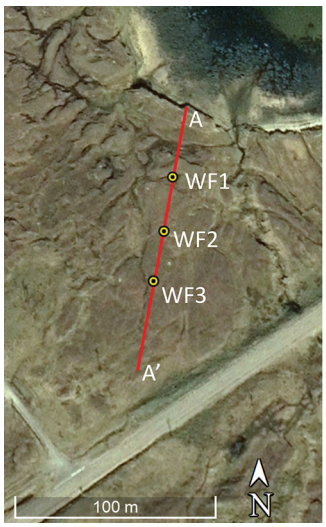

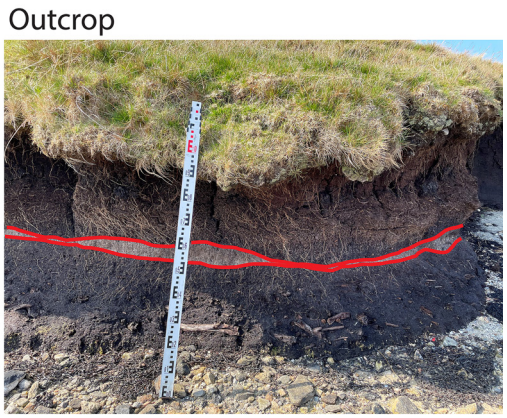

Fig. 6. Left: satellite image of Whale Firth showing the locations of the ground-penetrating radar profile and boreholes WF1, WF2 and WF3. Right: outcrop photograph of the pale-coloured tsunami sand layer within peat exposed in a low cliff at Whale Firth. The survey staff is just over 1 m in length. Lateral changes in the thickness of the tsunami sand layer are picked out by red lines at the contact between the sand and peat. Source: Google Earth™, image © 2023 CNES/ Airbus.

Grimister, but no results were reported. Given the known outcrop of tsunami sand at the head of Whale Firth and the orientation of the valleys, it seemed probable that there should be tsunami sands preserved at Grimister. Two GPR profiles were taken on either side of the river, *c.* 150 m inland from the beach. The GPR data at Grimister form a 140 m profile across the valley, divided into two sections by the Burn of Buster. Line A on the eastern side of the river is 60 m long and line B on the western side is 75 m long (Fig. 7). Antenna frequencies of 100 and 200 MHz were used, with a step size of 0.2 m and an antenna separation of 1 m. Auger boreholes G1 and G2 were made at 33 and 50 m on the GPR profile on the eastern side of the burn; borehole G3 is at 98 m on the western side of the burn.

Results

Ayre of Dury

All the profiles collected at the Ayre of Dury show two high-amplitude reflections across the entire profile, shown in red and brown in the GPR data (Fig. 8). The reflection shown in red indicates changes in dip across the profile and is interpreted as the tsunami sand. The reflection shown in brown suggests a more uniform dip from SE to NW (Fig. 8) and is interpreted as the contact between the base of the peat and the top of the underlying glacial deposits. A 3D model of the tsunami layer was also created and coloured by depth beneath the surface (Fig. 9). The depth of the tsunami sand layer varies from 1.1 m in the west to 0.3 m in the east and thus appears to be shallower towards the valley margin.

Basta Voe

The GPR line Basta A–B follows the coastline at Basta Voe and, as a result, has a slight bend to follow the outcrop. The data shows three strong reflections (Fig. 10). The base reflection (shown in brown) has a relatively high relief, between 2 and 4 m beneath the surface, between 0 and 70 m, before it disappears off the bottom of the data. The second reflection (shown in red) is almost continuous across the whole profile, except for a small gap between 98 and 105 m; it changes in elevation less than the basal brown reflection. A third strong reflection (shown in purple) occurs between 57 m, where it truncates against the reflection shown in red, and the end of the profile. There are a few small gaps in this reflection at 77–79, 90–93 and 98–105 m. This last gap corresponds to the gap in the reflection shown in red. A weak reflection is recorded beneath the reflection shown in red between 20 and 25 m (shown in pale blue). There are also multiple hyperbolas at 10 m along the profile (highlighted in yellow). These are created by noise from the telegraph pole and overhead wires located there. The reflection shown in brown is interpreted as the top of the glacial deposits/base peat. The reflection shown in red is correlated with a tsunami sand layer exposed along the coast (described by Dawson *et al.* 2006). The weak reflection shown in pale blue might correspond with thin sand layers of limited extent, which are possibly storm deposits (Dawson *et al.* 2006). The reflection shown in purple might be from a sand layer or a change in peat facies potentially forced by some other environmental event. Additional fieldwork is required to check these suggestions.

The Basta C line is perpendicular to the coastline and is 27.5 m long (Fig. 11). The data show one strong reflection (shown in red) that crosses the entire profile. At the start of the profile, away from the coast, this reflection is at an elevation of 2.8 m, whereas at the end of the profile, nearest the sea, it is at an elevation of 1.6 m. The results

Fig. 7. There is no outcrop at Grimister. The ground-penetrating radar profile is oriented east–west across the valley floor on boggy ground on both sides of the Burn of Buster, which drains north across the beach and into Whale Firth. Source: Google Earth™, image © 2023 CNES/Airbus.

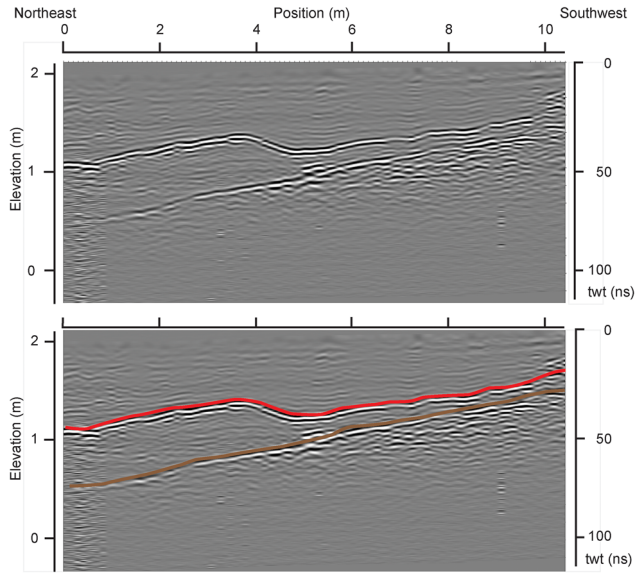

Fig. 8. Example of ground-penetrating radar data from the Ayre of Dury. The 3D survey data were collected along line F with 500 MHz antennas and closely spaced lines 0.5 m apart and 10 m long. The lower reflection (shown in brown) is interpreted as the contact between peat and glacial deposits. The red line shows the reflection from the tsunami sand, which appears to erode down into the peat.

from auger boreholes along the line of section are shown in Table 2. The depth to the sand layer increases inland and the thickness of the sand layer decreases inland. In addition, the sand layer becomes more diffuse inland, changing from sand to sandy peat.

Scatsta Voe

Figure 12 shows the results for the Scatsta A–A′ profile repeated with different antenna configurations. All have an SEC2 gain, an applied dewow and a topographic correction with the same topographic data as the surface (shown by a green line; Fig. 12). A high-amplitude reflection (shown in red) can be seen on all four profiles between 0 and 12 m and then again between 24 and 37 m along the line. This reflection is correlated with the tsunami sand outcrop in the waterfall, which is close to the start of the GPR profile. There is a concave-shaped 'bite' (shown by a dotted yellow line) between 12 and 24 m where the red reflection is missing (Fig. 12). Scatsta A.2, Scatsta A.3 and Scatsta A.4 have a second reflection (shown in brown) below the first reflection. This second reflection starts at 0 m and ends at 32 m on the Scatsta A.2 and Scatsta A.3 profiles, whereas it crosses the whole profile on Scatsta A.4. The lower reflection (shown in brown) is interpreted as the base of the peat/top-glacial. The absence of the brown reflection in the Scatsta A.1 line is due to attenuation of the 500 MHz signal, which was unable to penetrate the full depth of the peat. The peat was imaged by the lower frequency 200 and 100 MHz profiles A.2, A.3 and A.4 (Fig. 12).

The GPR profile Scatsta B–B′ is shown in Figure 13, with details in the lower panels (Fig. 13a, b, c). The GPR profile shows a continuous reflection at a depth of *c.* 2–3 m, which is actually two reflections coloured red and brown in Figure 13a, c. A third continuous inclined reflection can be seen between 100 and 140 m (coloured orange in Figure 13a, c).

Borehole Scatsta 1 at 108 m on GPR profile B–B′ has a total depth of 2.8 m and stopped when it was not possible to penetrate any deeper with the auger. From the top down, the stratigraphy is 0–2.49 m peat with a change in the character of the peat from an orange–brown rooted peat to finer grained dark brown peat from 1.84 to 1.9 m. A coarse-grained sand layer was present at 2.49–2.59 m (Fig. 13) and then a further 0.2 m of peat, terminating at 2.8 m.

Borehole Scatsta 2 at 175 m on GPR profile Scatsta B–B′ has a total depth of 2.2 m and stops where the auger hit a rock. The stratigraphy from the top down is 0–2.08 m peat, 2.08–2.15 m sand and 2.15–2.2 m peat (Fig. 13).

The reflection shown in brown (Fig. 13) is interpreted as the base of the peat/top-glacial. The red reflection is correlated with the tsunami sand layer sampled in borehole Scatsta 1. The orange reflection is correlated with a change in the character of the peat that was noted in borehole Scatsta 1.

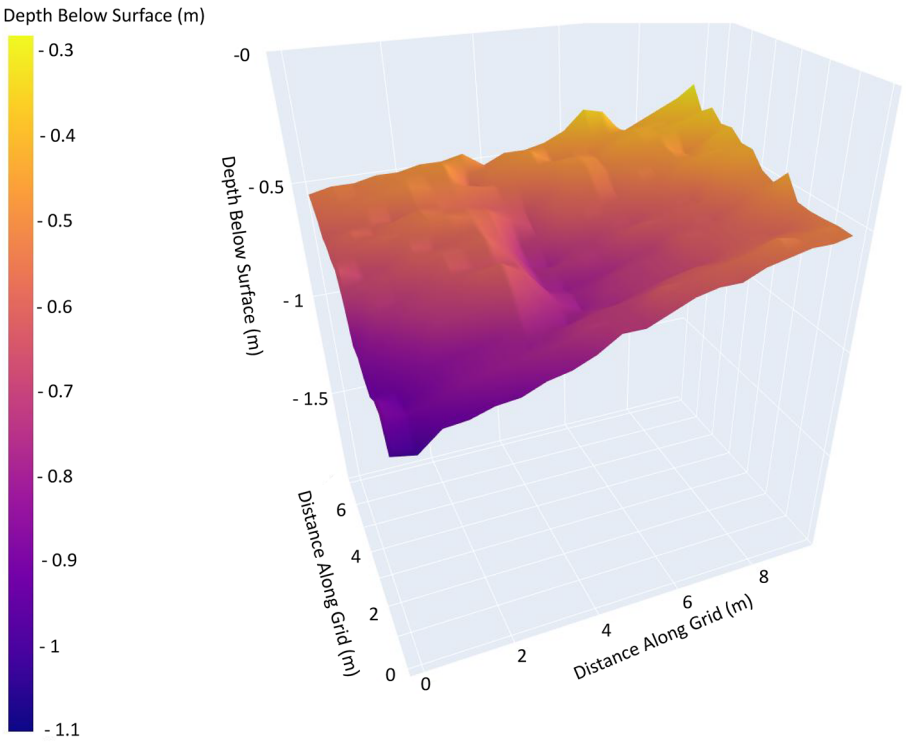

Fig. 9. 3D representation of the sand layer at Ayre of Dury. The colour scale shows the deepest part in purple and the shallowest area in yellow. The surface slopes from top right to bottom left (east–west) across the valley, with a depression in the middle that resembles a crescent-shaped scour, suggesting an erosive flow from left to right (inland).

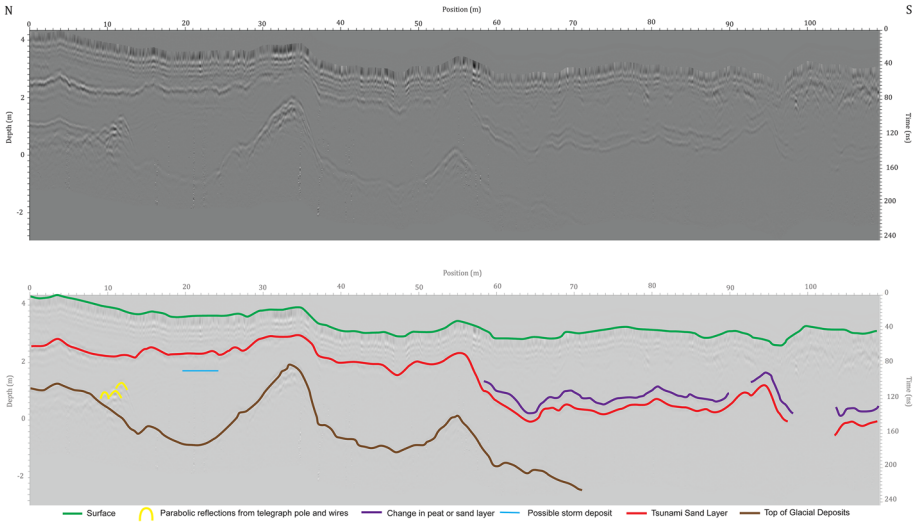

Fig. 10. Profile A–B at Basta Voe collected with 200 MHz antennas. The section shows a high-amplitude basal reflection with relatively high relief (brown), a continuous high-amplitude reflection in the mid-section with less relief (red) and a third reflection (purple) restricted to the eastern half of the profile where the section is thicker and the basal reflection (brown) disappears off the bottom of the data. The reflection shown in brown is interpreted as the top-glacial/basal peat reflection. The reflection shown in red correlates with the tsunami sand layer seen in outcrop. The reflection shown in purple is potentially from a change in peat facies, but appears to be laterally restricted to lower elevations in the eastern half of the profile.

Whale Firth

The three auger boreholes at Whale Firth all encountered sand layers within peat. Borehole WF 1 at 45 m along the GPR profile showed a 3 cm thick sand layer at a depth of 2.7 m and hit the base of the peat at 3.8 m. Borehole WF 2 at 77 m on the GPR profile encountered a 7 cm thick sand layer at 2.61–2.68 m, with the base of the peat at 3.05 m. Borehole WF3 at 110 m along the GPR profile encountered a 1 cm layer of fine sand with mica and 2 mm quartz granules at 2.5 m depth, with the base of the peat at 3 m. The GPR data collected at Whale Firth can be seen in Figure 14. There is a continuous reflection (shown in red) across the entire profile *c.* 2.5 m below the

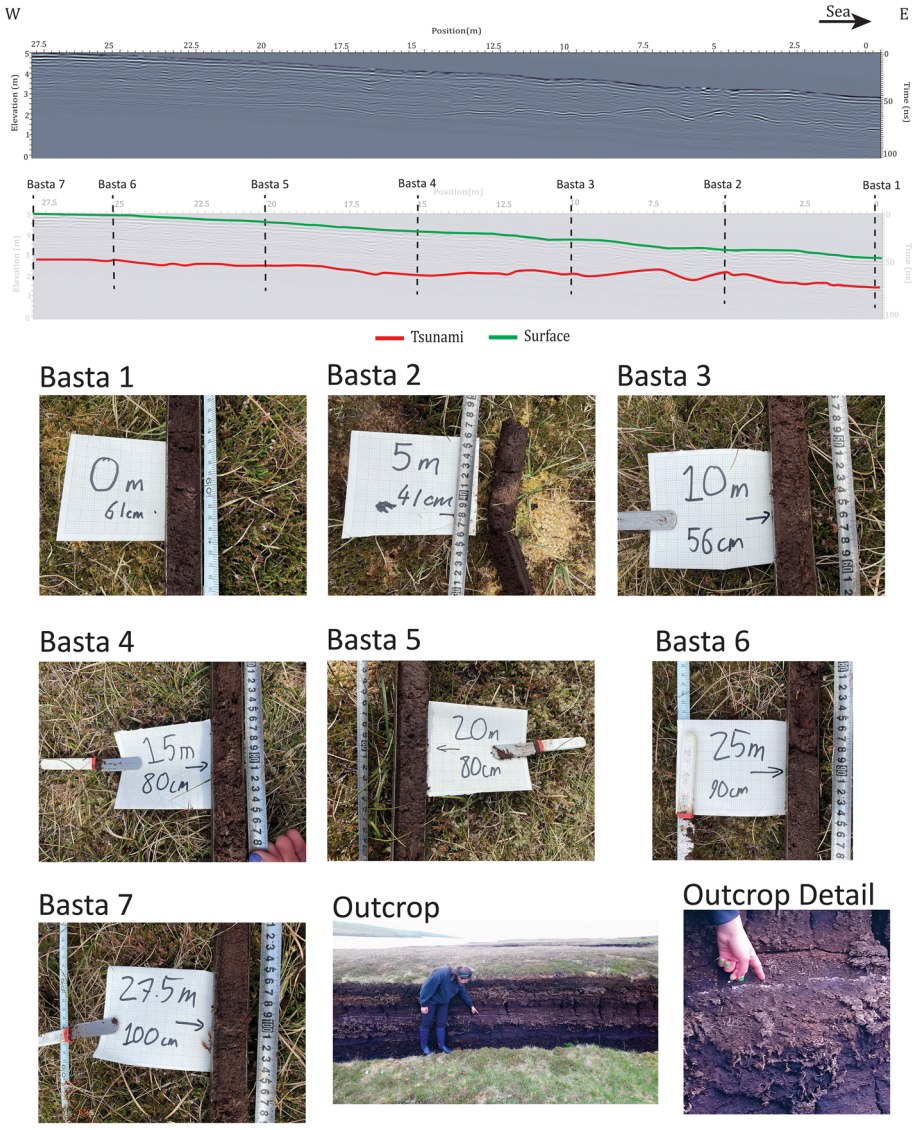

Fig. 11. Profile C–C′ at Basta Voe collected perpendicular to the coast with 500 MHz antennas. The tsunami sand layer is shown in red and corelated with auger boreholes. The depth to the sand layer varies from 1.0 m at 27.5 m to 0.41 m at 5 m. The sand layer varies in thickness between 1.5 cm and 2 mm, but is still visible across the ground-penetrating radar profile.

Table 2. Depth and thickness of sand layer from auger boreholes along the ground-penetrating profile Basta C–C′

Borehole	Distance along profile (m)	Depth to sand (m)	Sand thickness (m)
1	0	0.61	0.01
2	5	0.41	0.015
3	10	0.56	0.01
4	15	0.8	0.006
5	20	0.8	0.002
6	25	0.9	0.003
7	27.5	1.0	0.002

surface. This reflection corresponds with the sand layer in boreholes WF 1, 2 and 3 and is interpreted as the tsunami sand. The red reflection does not follow the surface topography and shows changes in amplitude along the profile. There is another, discontinuous, reflection (shown in brown) between 0.5 and 1 m below the first reflection, which is interpreted as the base of the peat/top-glacial. The upper (red) reflection follows the topography of the lower (brown) reflection and the two reflections become closer together up-slope, appearing to merge at *c.* 140 m, close to 10 m elevation.

Grimister

The GPR profile across the valley at Grimister was collected with the 200 and 100 MHz antennas. The results shown here are from the 100 MHz antennas, which achieved slightly greater depths of penetration (Fig. 15). The GPR profile is divided into two by the Burn of Buster, which runs along the valley floor. Three reflections are picked on the eastern side of the burn. The lowest reflection (shown in brown) is a continuous high-amplitude reflection that dips from just beneath the surface on the valley margin to a depth of −6 m at 40 m. The reflection shown in brown is interpreted as the base of the Holocene valley fill. Two gently inclined continuous reflections within the valley fill are marked by red lines on Figure 15. The reflections shown in red are interpreted as possible sand layers.

The base of the valley fill is less obvious on the western side of the river and is picked at a change in reflection character between the continuous sub-horizontal reflections and packages of discontinuous hyperbolic reflections. The continuous sub-horizontal reflections are interpreted as Holocene peat with sand layers. The discontinuous hyperbolic reflections are interpreted as boulders on the underlying glacial sediments.

Low-angle inclined reflections (shown in blue) are visible at the base of the valley fill and at 1.5 m beneath the surface between 70 and 90 m. There are also two small hyperbolas (shown in yellow). Curve-fitting to the hyperbolas indicates a velocity of 0.035 m/ns. The hyperbolic reflections are interpreted as buried objects. The low-angle inclined (pale blue) reflections are interpreted as river deposits.

The auger borehole G1 at Grimister has a total depth of 2.81 m and is mostly peat with two sand layers: a 3 cm sand layer at 0.9 m and a sand layer at 2.7 m, just above the base of the borehole at 2.81 m, where the auger hit a rock. Auger borehole G2 has a total depth of 3.3 m, which is mostly peat with multiple sand layers between 0.46 and 0.89 m, with a thin sand layer at 2.05 m and a

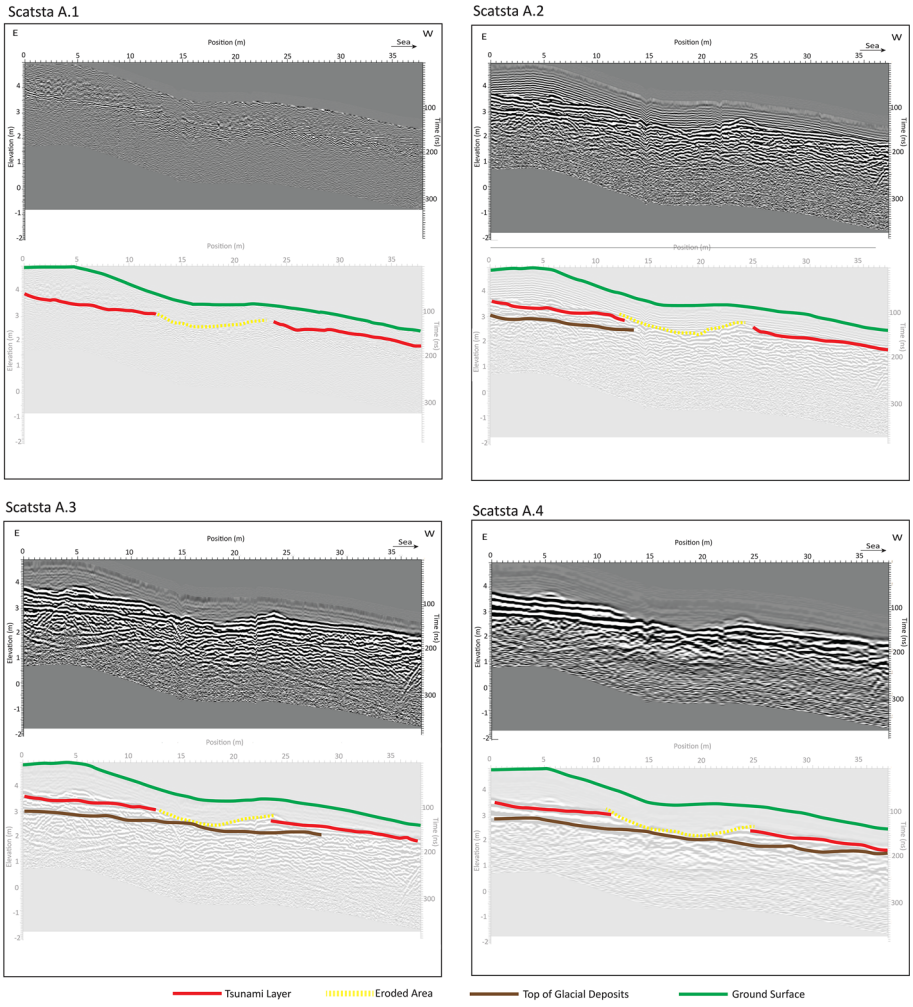

Fig. 12. Profiles A–A′ at Scatsta. Profile A.1 was collected with 500 MHz antennas and used a step size of 0.1 m and a separation of 0.23 m. Profile A.2 was collected with 200 MHz antennas and used a step size of 0.1 and a separation of 0.5 m. Profile A.3 was collected with 200 MHz antennas and used a step size of 0.2 m and a separation of 1 m. Profile A.4 was collected with 100 MHz antennas and used a step size of 0.25 m and a separation of 1 m. The ground surface is shown by the green lines. The reflection shown in red is interpreted as the tsunami sand layer and the line shown in brown is interpreted as the reflection from the base of the peat. The 200 MHz antennas with 1 m separation and a step size of 0.2 m (A.3) appear to give the best balance of penetration and resolution and this set-up was used for most of the ground-penetrating radar surveys.

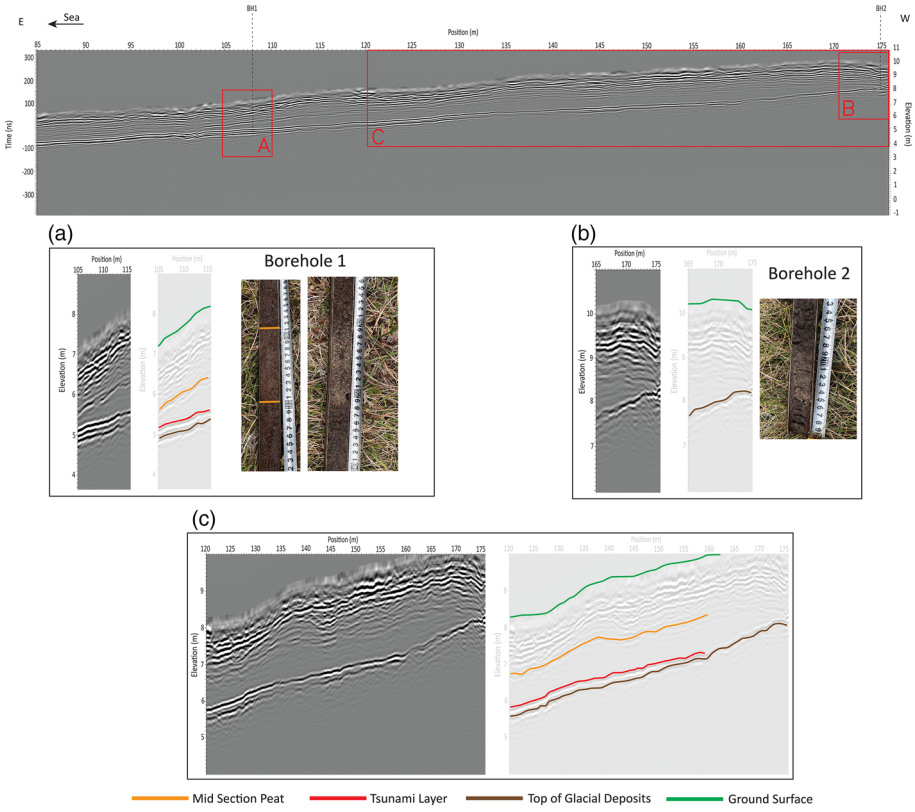

Fig. 13. Borehole and ground-penetrating radar data from the Scatsta B–B′ profile. The profile is 90 m long and located on the landward side of the B9076 road. Note that the reflection shown in red, interpreted as the tsunami sand, merges with the basal peat/top-glacial reflection (shown in brown) between 150 and 160 m in part (c), even though the sand layer is still found in borehole 2 at 175 m, shown in part (b), where there is only one reflection.

10 cm sand layer at 3.00 m. Borehole G3 has a total depth of 1.09 m with peat and thin sand layers. The two reflections shown in red appear to correlate with the sand layers between 0.46 and 0.9 m and the sand layer at 3.0 m. Because this profile was collected with 100 MHz antennas with a spacing of 1 m, it is not possible to discriminate the thin sand layers in the first metre of the section because this is obscured by the direct transmission between the transmitting and receiving antennas.

Discussion

GPR proved to be an excellent tool to map tsunami deposits in the shallow subsurface of the Shetland Islands. This is, in part, attributed to the contrast in dielectric permittivity of sand and peat, which produces clear reflections, even with relatively thin layers. In addition, there are few other subsurface features within the peat that might create similar reflections to the sand layers, as well as very

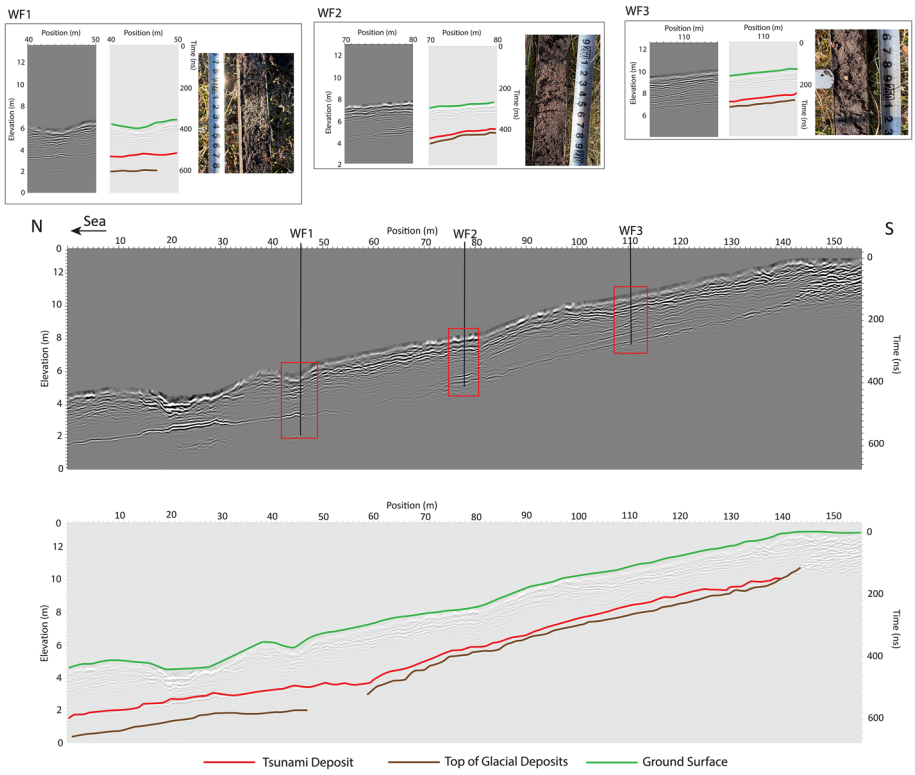

Fig. 14. Ground-penetrating radar profile at Whale Firth. The profile extends up-slope from the coast and the base of the peat is picked as a brown line, with the tsunami sand layer shown in red. The reflection from the tsunami sand layer changes amplitude and continues inland between 130 and 140 m and up-slope to 10 m elevation. The inset photographs show the tsunami sand layer in auger borehole cores: WF1 at 45 m along the profile; WF2 at 77 m; and WF3 at 110 m.

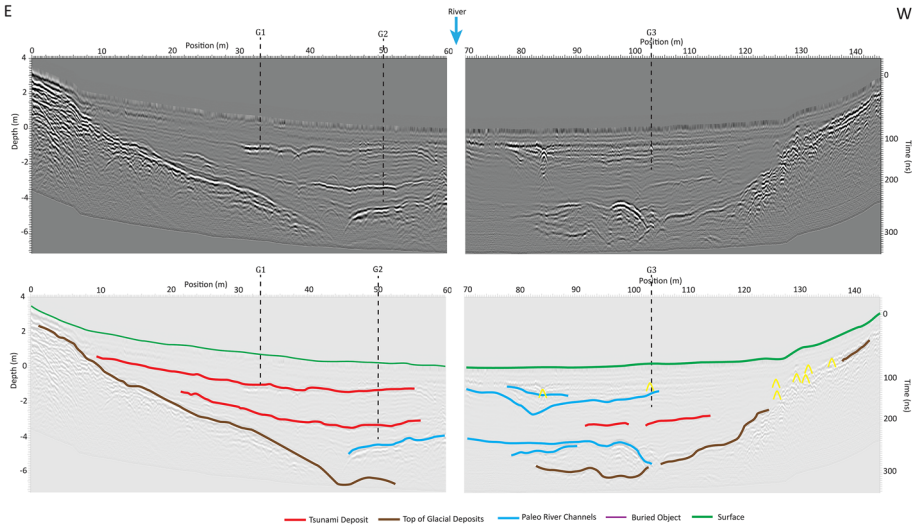

Fig. 15. Ground-penetrating radar profile across the valley at Grimister. The base of the Holocene valley fill is marked by the brown lines. The reflections interpreted as candidate tsunami sand layers are shown as red lines. Possible fluvial deposits are shown in pale blue and a hyperbolic reflection from a buried object is marked in yellow.

little electromagnetic noise from external sources. All of these factors contribute to our high-quality results. Furthermore, the ground conditions in the Shetland Islands are very good. At the time of the surveys, the ground was almost fully saturated with fresh rainwater, meaning that the water table was effectively at the surface and conductivity was low. Good contact between the antennas and the ground were assured using the ski-type antennas. Reflections attributed to changes in the peat facies were found at Scatsta B–B′ and possibly Basta Voe A–B and the ground truth from boreholes was helpful in confirming that the reflections are from sand layers.

GPR range and resolution of tsunami sand layers

In GPR surveys, there is a trade-off between the range, depth of penetration and resolution (Jol and Bristow 2003; Neal and Roberts 2000). GPR successfully imaged tsunami sand layers at each of the study sites, although different antennas were used at different locations. The thickness of the sand layers recorded from auger boreholes in this study varied from 0.1 m at Scatsta to 0.001 m in Basta C–C′. Different frequency antennas were tested at Scatsta A–A′, where the 100, 200 and 500 MHz antennas successfully imaged the sand layer, but the base-peat reflection was not visible on the profile from the 500 MHz antennas. The 200 MHz antennas were therefore selected for surveys at Scatsta and all the other sites because they provide a good trade-off between depth of penetration and resolution. However, the 500 MHz antennas were deployed to test the resolution of a very thin (>1 mm) sand layer at Basta Voe C–C′ and the 100 MHz antennas were used in addition to the 200 MHz antennas at Grimister, where the depth to the base-peat was greater, with a maximum depth of *c.* 6 m.

Thin beds

The GPR profiles imaged sand beds that were much thinner than we expected would be detected. Typically, the greatest vertical resolution that can be expected on a GPR profile is one-quarter of the wavelength (Widess 1973). The survey undertaken at Whale Firth was expected to have a minimum resolution of 0.04 m; however, a layer only 0.01 m thick was imaged with the 200 MHz antennas. Sand layers of 0.002 m were imaged at Basta Voe (line C–C′) using the 500 MHz antennas, which have a wavelength of 0.066 m, giving a theoretical resolution of 0.0165 m.

This is a good example of thin bed effects and there are several reasons why this is possible. The GPR antennas have nominal frequencies of 100, 200 and 500 MHz, but these are central frequencies and the signals transmitted have a bandwidth that includes higher and lower frequencies. Reflection of the higher frequency signal with a shorter wavelength can explain some of the thin bed effects (Guha *et al.* 2005). In addition, Zhou (2014) found that reflections from the top and bottom of thin beds can combine through constructive interference when the thickness is just one-eighth of the wavelength, which is close to the situation at Whale Firth and Basta Voe C–C′.

There is a contrast between the dielectric permittivity of peat and sand, which causes the reflections. Gourmanis *et al.* (2015) found that it is difficult to resolve thin beds when their dielectric properties are similar. The lack of any other layers within the peat may also help. Alternative explanations, such as signal tuning with constructive interference from repeating thin layers (Guha *et al.* 2005, 2008), appears unlikely due to the limited number of sand layers, commonly only one. It appears that a combination of signal tuning, where the higher frequency component of the transmitted signal is reflected, and constructive interference from the top and bottom of thin sand layers (Zhou 2014) is the most likely explanation for the imaging of sand layers thinner than the theoretical resolution of the GPR (calculated as a fraction of the wavelength of the central frequency of the transmitting antennas). Spectral analysis of the reflected signal and numerical modelling of electromagnetic wave propagation through layers of different thicknesses with the dielectric properties of peat and thin sand beds might help to determine the effects of bed thinning on signal tuning.

Amplitude

At Whale Firth, the amplitude of the reflection shown in red, which is confirmed as the tsunami sand in boreholes WF1, 2 and 3, changes along the profile (Fig. 14). The amplitude increases between 20 and 30 m along the profile and again at *c.* 45 m, where borehole WF1 is located. In the outcrop along the coast at Whale Firth, the sand layer shows changes in thickness from 0.12 to 0.01 m (Fig. 6) and it is possible that changes in the amplitude of the reflection could be associated with changes in the thickness of the sand layer. However, it is notable that the amplitude increases where there is a depression in the topography and where the ground is saturated (e.g. between 20 and 30 m). The increases in amplitude of the reflection from the tsunami sand layer might be due to the reduced thickness of the overlying peat within the depression, or the water content of the peat at the surface resulting in better ground contact and improved signal transmission into the ground. The borehole data were not sufficient to test these hypotheses, but changes in the amplitude of the reflection may be due to environmental factors (e.g. the water content of the peat and the

near-surface conditions), leading to increased signal transmission, and not necessarily due to the thickness of the tsunami sand.

Missing sections

One of the advantages of a GPR survey over investigations using boreholes alone is that GPR provides almost continuous profiles of the shallow subsurface, whereas the spacing between boreholes leaves gaps in the area of investigation (Takeda *et al.* 2018; Switzer *et al.* 2020). The tsunami sand forms a continuous reflection at most locations in the Shetland Islands. However, gaps have been recorded at Scatsta and at Basta Voe A–B. Possible explanations for a lack of reflections include non-deposition or erosion of the sand layers.

At Scatsta A–A′, the reflection interpreted to be the tsunami sand layer has a section missing between 12 and 22 m, indicated by a dashed yellow line in Figure 12. Potential causes of erosion of the sand layer at Scatsta were discussed by Bristow and Buck (2021). These include anthropogenic activity (e.g. peat cutting), stream erosion, tsunami erosion or peat slides. Of these, stream erosion appears to be the most likely and this is supported by the recent erosion by an unnamed stream adjacent to the section at Scatsta. On the GPR profile Basta Voe A–B, the reflections shown in red and purple both have a gap between 98 and 105 m that is coincident with lowering of the surface elevation (Fig. 10). This gap in both reflections at Basta Voe A–B implies that an erosive process has occurred here, most likely a small stream that has eroded down into the peat within a depression and removed the deposits of both sand layers.

This missing sections at Scatsta and Basa Voe are relatively small (10 and 7 m, respectively) and make up <10% of the survey length at each site, but highlight how the preservation of deposits can vary over small areas. A lack of tsunami sand layers due to the erosion of tsunami deposits by streams could result in the misinterpretation of borehole records. As a result, borehole records along stream sections should be treated with caution.

Buried topography

In the 3D survey at the Ayre of Dury, the reflection from the top-glacial/base-peat has a uniform inclination (Fig. 8), whereas the reflection from the tsunami sand layer has a lower angle dip and there is a change in dip in the middle of the survey line, creating a trough (Fig. 9). As a result, the topography of the tsunami sand layer does not correspond with the underlying base of the peat or with the surface. Two hypotheses can explain the trough in the middle of the sand layer. In hypothesis 1, the trough is caused by erosion beneath the tsunami sand layer caused by the tsunami. In hypothesis 2, the tsunami sand layer drapes across a pre-existing topography formed earlier due to the compaction of peat or erosion by a small stream. For hypothesis 1, erosion from the tsunami requires that it had at least two waves. The first wave caused erosion of the peat, creating the trough-like scour feature seen in the deposit in the underlying peat. The second wave then deposited the sand that created the tsunami deposit, forming a relatively uniform layer of sand that fines and thins inland (Bondevik *et al.* 2005). In hypothesis 2, the tsunami caused minimal erosion and deposited a relatively uniform deposit, preserving the pre-tsunami topography.

It is not possible from the GPR data alone to determine whether the increase in depth of the tsunami sand reflection at the Ayre of Dury is due to erosion by the tsunami or whether the topography existed before the tsunami and was simply draped by tsunami sand. However, the depression resembles a comet-shaped scour and its orientation suggests erosion by a current flowing inland towards the south, consistent with a tsunami flow. Erosion by the tsunami (hypothesis 1) is possible, but not proven, given that the shape of the depression in the middle of the survey is consistent with a hydraulic scour and that the field description of the Dury Voe event reports a sharp base, although without evidence for rip-up clasts (Bondevik *et al.* 2005).

The present day surface topography at Basta Voe does not follow the topography of the underlying glacial deposits. In addition, the depth to the tsunami sand layer increases inland at Basta C–C′. The increased thickness of peat inland along Basta Voe C–C′ is attributed to slower rates of peat accumulation approaching the coast, where there is increased drainage from the cliff and reduced peat preservation in the drier conditions. This observation shows that the accumulation of peat is not uniform over the area, most likely growing at a faster rate in the depressions in the ground where water gathers. This is supported by the changing depths of the sand layer and basal peat reflections at Basta Voe A–B, where the changes in elevation of the tsunami sand follow the general pattern of peaks and troughs on the top-glacial deposits, but with much gentler slopes. Here, the thickness of peat between the tsunami sand layers is greater over the troughs and thinner over the peaks (Fig. 10). A greater thickness of peat within the troughs supports increased peat formation and preservation within the troughs than over the peaks, most likely due to the local drainage conditions.

Distance inland

At Whale Firth, the reflection from the tsunami sand layer can be traced inland for 110 m and up to an elevation of 10 m (Fig. 14). At Scatsta B, the reflection from the tsunami sand can be traced *c.* 160 m inland and up to an elevation of 7 m OD (Fig. 13). In both cases, the inland limit of the tsunami reflection appears to merge with the underlying base-peat reflection. The borehole Scatsta 2 at 175 m on GPR profile B–B′ shows that the sand layer was still present as a 7 cm layer 15 m beyond the limit of the tsunami sand reflection. Given that the wavelength of the 200 MHz antennas is *c.* 0.17 m with a resolution of 0.04 m, it should be possible to distinguish the 7 cm sand layer and the 15 cm peat beneath it. However, the two horizons appear to merge into one reflection because the wavelength is similar to the spacing between the sand layer and the base of the peat.

The inland limits of the tsunami sand layers clearly extend beyond the limits defined by GPR alone. The thickness of the peat between the tsunami sand and the basal reflection is important in aiding the discrimination of a tsunami sand layer, as seen at Scatsta B and Whale Firth. The reflections merge as the thickness of the peat layer between the tsunami sand and the base of the peat approaches the wavelength of the antennas. This limits the ability to discriminate sand layers with GPR at Scatsta and Whale Firth beyond 160 and 110 m, respectively. Previous boreholes at Scatsta reported by Smith *et al.* (2004) show that the inland extent of the tsunami sand at Scatsta is at least 250 m, 90 m beyond the limit apparent on GPR.

Run-up

Outstanding issues in estimating the wave run-up from the Storegga tsunami in the Shetland Islands include uncertainty in the estimates of sea-level at the time of the tsunami and the extent to which the waves extend beyond the limits of sand deposition (Dawson *et al.* 2020). There is limited data to constrain Holocene sea-levels around the Shetland Islands and Bondevik *et al.* (2005) concluded that the sea-level at the time of the Storegga slide was at least 10–15 m lower than at the present day. The latest estimates by Dawson *et al.* (2020) use a value of −20 m as a realistic estimate.

The sand layer at Scatsta is attributed to the Storegga tsunami that occurred more than 8000 years ago and the reflection on the GPR records the sand layer at 7 m elevation. Dawson *et al.* (2020) suggest

that 20 m is a realistic estimate for the change in sea-level since then, indicating a run-up of *c.* 27 m.

The sand layer at Whale Firth can be traced to an elevation of 10 m above OD on the GPR profile (Fig. 14) and the sand layer is dated at 4.760 ± 0.030 cal ka BP (Tappin *et al.* 2015). However, this age is not conclusive and Dawson *et al.* (2020) infer that the sand layer was deposited from the Storegga tsunami rather than the Garth tsunami. If the sand layer at Whale Firth was deposited by the Storegga tsunami, then 20 m should be added to the run-up. If it was deposited by the Garth tsunami, then sea-level rise will have been close to 9 m in the 5000 years since then. Depending on the age of the sand layer, a sea-level rise of 20 m or 9 m must be added to any run-up height found by the GPR data. In addition, it is important to remember that the wave run-up exceeds the extent of the sand layer and therefore this only represents a minimum run-up height (Abe *et al.* 2012). Taking account of the change in sea-level since the tsunami, combined with the elevation of the sand layers at Whale Firth, leads to a minimum wave run-up of 19 m and possibly 30 m. The complex bathymetry around the islands and the narrow inlets and channels between the islands will generate local focusing of waves and increases in wave height in some areas, but also shelter with lower wave heights in other areas where the waves break offshore.

Multiple events recorded at Grimister

The sites at Whale Firth and Grimister lie within the same inlet, with Grimister nearest the open ocean and the outcrop at Whale Firth at the furthest end of the inlet. The GPR data show evidence of two possible sand layers at Grimister, but only one at Whale Firth. Because the tsunami at Whale Firth has been tentatively dated to the mid-Holocene Garth tsunami, this event must also have impacted Grimister. However, there is no dating information for the deposits at Grimister and we speculate that the reflections here could originate from sand layers from tsunamis or mega-storms. Radiocarbon dating of the peat deposits and detailed sedimentary analysis of the sand layers are required to constrain the age and likely origins of the reflections interpreted as potential tsunami deposits at Grimister.

Wider implications

Although we have shown that GPR can be used to determine the extent of sand layers attributed to tsunami events, we were not able to use GPR to distinguish between sand layers that were deposited by tsunami from sand layers that might have been deposited by mega-storms. GPR lacks the resolution to identify the variations in grain size and sedimentary structures that might allow a distinction between mega-storm events and tsunamis. However, the identification of a crescent-shaped scour at Dury Voe suggests a sustained onshore erosive current, which is more likely to occur during a tsunami than during a storm event. Either way, the occurrence of extensive, water-lain sand sheets of marine origin deposited by mega-storms and tsunamis represent a significant coastal hazard. In this respect, the approach used here could be extended to search for wash-over deposits from major storms (including hurricanes, cyclones and typhoons), where sand layers are preserved, especially within peat-forming environments such as coastal wetlands and swamps.

Tsunami impact

The sea-level at the time of the Storegga slide (*c.* 8000 years ago) was lower than it is today. The sea-level is poorly constrained as a result of uncertainties over the post-glacial isostatic uplift of the Shetland Islands and a lack of dated Holocene sea-level indicators. However, it is accepted that the sea-level would have been 10–15 m lower than today (Bondevik *et al.* 2005) or −14 to −20 m (Dawson *et al.* 2020). This needs to be considered when assessing the impact should such an event occur today. The mainstays of the economy of the Shetland Islands are oil and gas, fishing and aquaculture, and tourism. All of these are largely, or almost entirely, coastal and therefore potentially vulnerable to a tsunami.

The height of the deposits at Scatsta Voe implies that inundation reached at least 7 m above the current sea-level. Smith *et al.* (2004) report sand within peat at an altitude of 11.8 m at Scatsta. Given that the change in sea-level since then is *c.* 20 m, this means that should a similar event happen now, the nearby Sullom Voe oil terminal would be impacted, with water levels reaching *c.* 20–30 m elevation. The Sullom Voe oil terminal is one of the largest oil terminals in Europe and receives oil via pipelines from the oilfields in the East Shetland Basin and the deep waters west of Shetland. Oil is then exported worldwide by tanker. The oil storage tanks at Sullom Voe are *c.* 30 m above sea-level and are surrounded by a bund, so they should be safe. However, the port facilities, offices, gas processing facilities and pipelines to the harbour are well within the zone of inundation (Bristow and Buck 2021). In addition, the airport at Scatsta and the nearby harbour at Sella Ness are at elevations of *c.* 10 and 1 m, respectively, placing them within the zone of inundation. Elsewhere around the Shetland Islands, critical infrastructure, such as the island's main airport at Sumburgh, is at *c.* 3 m OD, as is the harbour and power station at Lerwick, the island's capital. In addition, all the ferry connections between the islands are potentially vulnerable.

Conclusions

Sand layers in peat are clearly resolved by GPR and tsunamigenic sands have been successfully imaged at all of the locations studied in the Shetland Islands due to the contrast in dielectric permittivity between peat and sand, helped by good ground conditions. Tsunami sand layers have been traced up to 140 m inland and 10 m above current sea-level on GPR profiles at Whale Firth and 150 m inland at 7 m elevation at Scatsta Voe. In both cases, the limitation of the inland extent of the reflection is the apparent merging of the tsunami sand reflection and the reflection from the base of the peat. This appears to be a limiting factor and underestimates the true extent of the sand sheets. At Scatsta, the sand sheet has been recorded further inland during a previous borehole survey (Smith *et al.* 2004). By contrast, the extent and elevation of the sand sheet at Whale Firth as recorded by GPR in this study are more extensive than reported in a previous study using boreholes alone.

The tsunami sand layers appear to drape the underlying topography, as seen at Basta Voe, while a 3D survey at Ayre of Dury revealed a crescent-shaped scour, likely formed by an inflowing tsunami. Post-depositional erosion, most likely by streams, can locally remove tsunami sand layers, as seen as Scatsta and Basta Voe. Missing sections caused by stream erosion could result in misinterpretation of the extent of sand sheets from borehole surveys. At Grimister, a site with no previous record of tsunami sands, the GPR reflections suggest the preservation of more than one tsunami sand layer; sand layers have been found within the peat using auger boreholes. These results show that GPR is a useful technique for mapping the extent of tsunamigenic sand layers and exploring for sand layers within areas with no exposure. Should such a tsunami event occur today, the infrastructure and economy of the Shetland Islands would be devastated.

Scientific editing by Gene Rankey

Acknowledgements The authors thank Maria Irene Inggrid for her help with data collection and the land-owners on Shetland for permission to survey the sites and collect borehole samples, and Dr Adam Booth, University of Leeds for the loan of 500 MHz antennas.

Author contributions

LB: funding acquisition (lead), investigation (lead), writing – original draft (lead), writing – review and editing (supporting); **CSB**: conceptualization (lead), supervision (lead), writing – review and editing (lead).

Funding

This work was funded by the Natural Environment Research Council (NE/L002485/1).

Competing interests

The authors declare that they have no known competing financial interests or personal relationships that could have appeared to influence the work reported in this paper.

Data availability

The GPR data described here are archived at the NERC Geophysical Data Repository.

References

Abe, T., Goto, K. and Sugawara, D. 2012. Relationship between the maximum extent of tsunami sand and the inundation limit of the 2011 Tohoku-oki tsunami on the Sendai Plain, Japan. *Sedimentary Geology*, **282**, 142–150, https://doi:10.1016/j.sedgeo.2012.05.004

Alhamid, A.K., Akiyama, M., Ishibashi, H., Aoki, K., Koshimura, S. and Frangopol, D.M. 2022. Framework for probabilistic tsunami hazard assessment considering the effects of sea-level rise due to climate change. *Structural Safety*, **94**, 102152, https://doi.org/10.1016/j.strusafe.2021.102152

Bondevik, S. and Svendsen, J.I. 1998. Distinction between the Storegga tsunami and the Holocene marine transgression in coastal basin deposits of western Norway. *Journal of Quaternary Science*, **13**, 529–537, https://doi.org/10.1002/(SICI)1099-1417(1998110)13:6<529::AID-JQS388>3.0.CO;2-1

Bondevik, S., Svendsen, J.I. and Mangerund, J. 1997*a*. Tsunami sedimentary facies deposited by the Storegga tsunami in shallow marine basins and coastal lakes, western Norway. *Sedimentology*, **44**, 1115–1131, https://doi.org/10.1046/j.1365-3091.1997.d01-63.x

Bondevik, S., Svendsen, J.I., Johnson, G., Mangerund, J. and Kaland, P.E. 1997*b*. The Storegga tsunami along the Norwegian coast, its age and runup. *Boreas*, **26**, 29–53, https://doi.org/10.1111/j.1502-3885.1997.tb00649.x

Bondevik, S., Mangerund, J., Dawson, S., Dawson, A. and Lohne, O. 2003. Record-breaking height for 8000-year-old tsunami in the North Atlantic. *EOS*, **31**, 289–300, https://doi.org/10.1029/2003EO310001

Bondevik, S., Mangerud, J., Dawson, S., Dawson, A. and Lohne, Ø. 2005. Evidence for three North Sea tsunamis at the Shetland Islands between 8000 and 1500 years ago. *Quaternary Science Reviews*, **14–15**, 1757–1775, https://doi.org/10.1016/j.quascirev.2004.10.018

Bondevik, S., Stormo, S.K. and Skjerdal, G. 2012. Green mosses date the Storegga tsunami to the chilliest decades of the 8.2 ka cold event. *Quaternary Science Reviews*, **45**, 1–6, https://doi.org/10.1016/j.quascirev.2012.04.020

Bristow, C. and Buck, L. 2021. GPR survey of Storegga tsunami deposits, Shetland Islands, UK and geohazard discussion. *Engineering and Mining Geophysics*, **2021**, 1–8, https://doi.org/10.3997/2214-4609.202152184

Coppola, D. 2020. *Introduction to International Disaster Management*. 4th edition, Elsevier, https://doi.org/10.1016/C2018-0-00377-1

Costa, P.J.M. and Andrade, C. 2020. Tsunami deposits: present knowledge and future challenges. *Sedimentology*, **67**, 1189–1206, https://doi.org/10.1111/sed.12724

Dawson, S. and Smith, D.E. 1997. Holocene relative sea-level changes on the margin of a glacio-isostatically uplifted area: an example from northern Caithness, Scotland. *The Holocene*, **7**, 59–77, https://doi.org/10.1177/095968369700700106

Dawson, A.G., Dawson, S. and Bondevik, S. 2006. A late Holocene tsunami at Basta Voe, Yell, Shetland Isles. *Scottish Geographical Journal*, **122**, 100–108, https://doi.org/10.1080/00369220600917404

Dawson, A.G., Dawson, S., Bondevik, S., Costa, J.M., Hill, J. and Stewart, I. *et al.* 2020. Reconciling Storegga tsunami sedimentation patterns with modelled wave heights: a discussion from the Shetland Isles field laboratory. *Sedimentology*, **67**, 1344–1353, https://doi.org/10.1111/sed.12643

Engel, M., May, S.M., Pilarczyk, J., Brill, D. and Garrett, E. 2020. Geological records of tsunamis and other extreme waves: concepts, applications and a short history of research. *In:* Engel, M., May, S.M., Pilarczyk, J., Brill, D. and Garrett, E. (eds) *Geological Records of Tsunamis and Other Extreme Waves*, Elsevier, 3–20, https://doi.org/10.1016/B978-0-12-815686-5.00001-8

Engel, M., Hess, K. *et al.* 2023. Sedimentary evidence of the Late Holocene tsunami in the Shetland Islands (UK) at Loch Flugarth, northern Mainland. *Boreas*, **53**, 27–41, https://doi.org/10.1111/bor.12635

Goto, K., Ikehara, K., Goff, J., Chagué-Goff, C. and Jaffe, B. 2014. The 2011 Tohoku-Oki tsunami – three years on. *Marine Geology*, **358**, 2–11, https://doi.org/10.1016/j.margeo.2014.08.008

Gourmanis, C., Switzer, A. *et al.* 2015. Ground penetrating radar examination of thin tsunami beds – a case study from Phra Thong Island, Thailand. *Sedimentary Geology*, **329**, 149–165, https://doi.org/10.1016/j.sedgeo.2015.09.011

Grauert, M., Bjorck, S. and Bondevik, S. 2001. Storegga tsunami deposits in a coastal lake on Suduroy, the Faroe Islands. *Boreas*, **30**, 300–9483, https://doi.org/10.1111/j.1502-3885.2001.tb01045.x

Guha, S., Kruse, S.E., Wright, E.E. and Kruse, U.E. 2005. Spectral analysis of ground penetrating radar response to thin sediment layers. *Geophysical Research Letters*, **32**, L23304, https://doi.org/10.1029/2005GL023933

Guha, S., Kruse, S. and Wang, P. 2008. Joint time–frequency analysis of GPR data over layered sequences. *The Leading Edge*, **27**, 1454–1460, https://doi.org/10.1190/1.3011017

Haflidason, H., Lien, R., Sejrup, H.P., Forsberg, C.F. and Bryn, P. 2005. The dating and morphometry of the Storegga slide. *Marine and Petroleum Geology*, **22**, 123–136, https://doi.org/10.1016/j.marpetgeo.2004.10.008

Hess, K., Engel, M. *et al.* 2023. A 1500-year record of North Atlantic storm flooding from lacustrine sediments, Shetland Islands (UK). *Journal of Quaternary Science*, https://doi.org/10.1002/jqs.3568

Jin, D. and Lin, J. 2011. Managing tsunamis through early warning systems: a multidisciplinary approach. *Ocean and Coastal Management*, **54**, 189–199, https://doi.org/10.1016/j.ocecoaman.2010.10.025

Jol, H.M. and Bristow, C.S. 2003. GPR in sediments: advice on data collection, basic processing and interpretation, a good practice guide. *Geological Society. London, Special Publications*, **211**, 9–27, https://doi.org/10.1144/GSL.SP.2001.211.01.02

Jol, H.M. and Peterson, C.D. 2006. Imaging earthquake scarps and tsunami deposits in the Pacific Northwest, USA. *Symposium on the Application of Geophysics to Engineering and Environmental Problems Proceedings*. 2–6 April, 2006, Seattle, WA, Environmental & Engineering Geophysical Society, 217–229, https://doi.org/10.4133/1.2923651

Kortekaas, S. and Dawson, A.G. 2007. Distinguishing tsunami and storm deposits: an example from Martinhal, SW Portugal. *Sedimentary Geology*, **200**, 208–221, https://doi.org/10.1016/j.sedgeo.2007.01.004

Koster, B. and Reicherter, K. 2014. Sedimentological and geophysical properties of a ca. 4000year old tsunami deposit in southern Spain. *Sedimentary Geology*, **314**, 1–16, https://doi.org/10.1016/j.sedgeo.2014.09.006

Koster, B., Hadler, H., Vott, A. and Reicherter, K. 2013. Application of GPR for visualising spatial distribution and internal structures of tsunami deposits? Case studies from Spain and Greece. *Zeitschrift für Geomorphologie, Supplementary Issue*, **57**, 29–45, https://doi.org/10.1127/0372-8854/2013/S-00151

Koster, B., Hoffmann, G., Grutzner, C. and Reicherter, K. 2014. Ground penetrating radar facies of inferred tsunami deposits on the shores of the Arabian Sea (northern Indian Ocean). *Marine Geology*, **351**, 13–24, https://doi.org/10.1016/j.margeo.2014.03.002

Li, L., Switzer, A.D., Wang, Y., Chan, C.H., Qiu, Q. and Weiss, R. 2018. A modest 0.5 m rise in sea level will double the tsunami hazard in Macau. *Science Advances*, **4**, eaat1180, https://doi.org/10.1126/sciadv.aat1180

Long, D., Barlow, N.L.M. *et al.* 2016. Lateglacial and Holocene relative sea-level changes and first evidence for the Storegga tsunami in Sutherland, Scotland. *Journal of Quaternary Science*, **31**, 239–255, https://doi.org/10.1002/jqs.2862

Minoura, K., Imamura, F., Sugawara, D., Kono, Y. and Iwashita, T. 2001. The 869 Jogan tsunami deposit and recurrence interval of large-scale tsunami on the Pacific coast of northeast Japan. *Journal of Natural Disaster Science*, **23**, 83–88, http://dl.ndl.go.jp/info:ndljp/pid/11150431

Neal, A. and Roberts, C.L. 2000. Applications of ground-penetrating radar (GPR) to sedimentological geomorphological and geoarchaeological studies in coastal environments. *Journal of the Geological Society, London*, **175**, 139–171, https://doi.org/10.1144/GSL.SP.2000.175.01.12

Parry, L.E., West, L.J., Holden, J. and Chapman, P.J. 2014. Evaluating approaches for estimating peat depth. *Journal of Geophysical Research: Biogeosciences*, **119**, 567–576, https://doi.org/10.1002/2013JG002411

Phantuwongraj, S. and Choowong, M. 2012. Tsunami versus storm deposits from Thailand. *Natural Hazards*, **63**, 31–50, https://doi.org/10.1007/s11069-011-9717-8

Premasiri, R., Styles, P., Shirira, V., Cassidy, N. and Schwenninger, J.-L. 2015. OSL dating and GPR mapping of palaeotsunami inundation: a 4000-year history of Indian Ocean tsunamis as recorded in Sri Lanka. *Pure and Applied Geophysics*, **172**, 3357–3384, https://doi.org/10.1007/s00024-015-1128-4

Proulx-McInnis, S., St-Hilaire, A., Rousseau, A.N. and Jutras, S. 2013. A review of ground-penetrating radar studies related to peatland stratigraphy with a case study on the determination of peat thickness in a northern boreal fen in Quebec, Canada. *Progress in Physical Geography: Earth and Environment*, **37**, 767–786, https://doi.org/10.1177/0309133313501106

Satake, K. and Atwater, B.F. 2007. Long-term perspectives on giant earthquakes and tsunamis at subduction zones. *Annual Review of Earth and Planetary Sciences*, **35**, 349–374, https://doi.org/10.1146/annurev.earth.35.031306.140302

Sawai, Y., Tamura, T., Shimada, Y. and Tanigawa, K. 2023. Scour ponds from unusually large tsunamis on a beach-ridge plain in eastern Hokkaido, Japan. *Scientific Reports*, **13**, 3064, https://doi.org/10.1038/s41598-023-30061-9

Smith, D.E. 1993. Norwick, Unst; Burragarth, Unst; Sullom Voe, Mainland. *In:* Birnie, J., Gordon, J., Bennett, K. and Hall, A. (eds) *The Quaternary of Shetland. Quaternary Research Association Field Guide*, 52–56.

Smith, D.E., Firth, C.R., Turbayne, S.C. and Brooks, C.L. 1992. Holocene relative sea-level changes and shoreline displacement in the Dornoch Firth area, Scotland. *Proceedings of the Geologists' Association*, **103**, 237–257, https://doi.org/10.1016/S0016-7878(08)80232-5

Smith, D.E., Shi, S. *et al.* 2004. The Holocene Storegga slide tsunami in the United Kingdom. *Quaternary Science Reviews*, **23**, 2291–2321, https://doi.org/10.1016/j.quascirev.2004.04.001

Switzer, A.D. and Jones, B.G. 2008. Large-scale washover sedimentation in a freshwater lagoon from the southeast Australian coast: sea-level change, tsunami or exceptionally large storm? *The Holocene*, **18**, 787–803, https://doi.org/10.1177/0959683608089214

Switzer, A.D., Gouramanis, C., Bristow, C.S. and Simms, A.R. 2020. Ground-penetrating radar (GPR) in coastal hazard studies. *In*: Engel, M., Pilarczyk, J., May, S.M., Brill, D. and Garrett, E. (eds) *Geological Records of Tsunamis and Other Extreme Waves*. Elsevier, 143–168, http://dx.doi.org/10.1016/B978-0-12-815686-5.00008-0

Takamura, M., Udo, K., Sato, M. and Takahashi, K. 2016. Analysis of coastal erosion due to the 2011 great east Japan tsunami and its recovery using ground penetrating radar data. *Journal of Coastal Research*, **75**, 477–481, https://doi.org/10.2112/SI75-096.1

Takeda, H., Goto, K., Goff, J., Matsumoto, H. and Sugawara, D. 2018. Could tsunami risk be underestimated using core-based reconstructions? Lessons from ground penetrating radar. *Earth Surface Processes and Landforms*, **43**, 808–816, https://doi.org/10.1002/esp.4282

Tappin, D., Long, D. and Carter, G.D.O. 2015. *Shetland Islands Field Trip May 2014: Summary of Results*. British Geological Survey, Nottingham, https://nora.nerc.ac.uk/id/eprint/510756/1/OR15017.pdf

ten Brink, U.S., Chaytor, J.D., Geist, E.L., Brothers, D.S. and Andrews, B.D. 2014. Assessment of tsunami hazard to the U.S. Atlantic Margin. *Marine Geology*, **353**, 31–54, https://doi.org/10.1016/j.margeo.2014.02.011

Tursina, T., Syamsidik, S. and Kato, S. 2022. Incorporating dynamics of land use and land cover changes into tsunami numerical modelling for future tsunamis in Banda Aceh. *E3S Web of Conferences*, **340**, 01014, https://doi.org/10.1051/e3sconf/202234001014

Wagner, B., Bennike, O., Klug, M. and Cremer, H. 2007. First indication of Storegga tsunami deposits from East Greenland. *Journal of Quaternary Science*, **22**, 321–325, https://doi.org/10.1002/jqs.1064

Widess, M.B. 1973. How thin is a thin bed? *Geophysics*, **38**, 1176–1180, https://doi.org/10.1190/1.1440403

Zhou, H. 2014. *Practical Seismic Data Analysis*. Cambridge University Press.